Transient response of IR detectors used in space astronomy : what we have learned from ISO satellite

Alain Coulais[a], Boris I. Fouks[b], Jean-François Giovannelli[c], Alain Abergel[a], Johann Sée[c,a]

[a]Institut d'Astrophysique Spatiale
Bâtiment 121, Université Paris XI, 91405 Orsay cedex, France
[b]Institute of Radio Engineering and Electronics of Russian Academy of Sciences,
11 Mokhovaya Str., GSP-3, Moscow, 103907, Russia
[c]Laboratoire des Signaux et Systèmes (CNRS-SUPÉLEC-UPS)
SUPÉLEC, Plateau de Moulon, 91192 Gif-sur-Yvette Cedex, France

ABSTRACT

Doped silicon and germanium bulks with implanted low ohmic contacts are extensively used as extrinsic photoconductors for infrared astronomy from ground based, balloon, airborne and space observatories. These detectors are characterized by temporal transient effects after flux change, which can bias the photometry by significant factors. A systematic correction of these effects can significantly reduce the observing time and improve the final accuracy.

A large number of such detectors were used on-board the Infrared Space Observatory (ISO) satellite. Detailed results have been obtained about transient effects (description, models, correction) from data taken both on the ground before the launch and on-board.

For most of the Si:Ga detectors of three instruments of ISO (CAM, PHT and SWS), the transient effects are qualitatively identical. For uniform illumination, the response is precisely described by one non linear model. The problem of non uniform illumination (especially point sources) is more complicated. Preliminary results with a tri-dimensional model are encouraging. On the other hand the Ge:Ga detectors (PHT and LWS on-board ISO) may have qualitatively different peculiarities. At the present time only empirical models properly reproduce them but with a limited exactness.

We present the physical and empirical models that are actually developed for the ISO detectors together with dedicated inversion techniques. The problems encountered with ISO detectors are obviously extremely useful in order to test and improve the Si and Ge detectors used in the future.

Keywords: Infrared Space Observatory (ISO), low-background IR detectors, extrinsic photodetectors, transient effects, crosstalk, inversion.

1. INTRODUCTION

The implementation of InfraRed (IR) detectors in space is strongly complicated by memory effects, which may have a strong amplitude due to the low brightness of the Universe at these wavelengths. For this reason these detectors exhibit very long-term transient currents under flux changes. The time allocated for the observation of an astronomical source is strictly restricted because of the large number of astronomical sources to be observed. Therefore it is not possible to wait for the current stabilization under the input flux then to determine it directly.

From the transient problem point of view, the ISO[28] satellite is a very interesting laboratory since several technologies (Ge:Be, Ge:Ga, In:Sb, CID In:Sb, Si:As, Si:Ga, Si:B)[8,32,12,14] have been used to cover an extended spectral range from 2.5 to 250 μm. Three years after the end of the mission, transient effects are still under study in order to increase the final sensitivity. Without any correction, the final error can be as large as 50 % for a block (several elementary observations (readouts) on the same position on the sky). However the response after flux change is highly reproducible which gives sense to look for models and to correct them.

Further author information : (Send correspondence to A. C.)
A. C. : E-mail : alain.coulais@ias.fr, B. F. : E-mail : bfoux@juno.com, J-F. G. : E-mail : giova@lss.supelec.fr, A. A. : E-mail : alain.abergel@ias.fr, J. S. : E-mail : see@rip.ens-cachan.fr.

	detector name	type	wavelength (μm)	pixels
CAM[8]	SW	CID In:Sb	2.5 – 5.5	32×32
	LW	Si:Ga	4. – 18.	32×32
PHT[32]	S1 & S2	Si:Ga	15, (peak)	two 1
	P1	Si:Ga	15. (peak)	1
	P2	Si:B	25. (peak)	1
	P3	Ge:Ga	100. (peak)	1
	C 100	Ge:Ga	100. (peak)	3×3
	C 200	Ge:Ga (stressed)	180. (peak)	2×2
SWS[14]	band 1	In:Sb	2.4 – 4.1	1×12
	band 2	Si:Ga	4.1 – 12	1×12
	band 3	Si:As	12. – 29.	1×12
	band 4	Ge:Be	29. – 45.2	1×12
	FP band 5	Si:Sb	11.4 – 26.	1×2
	FP band 6	Ge:Be	26. – 44.5	1×2
LWS[9,12]	SW1	Ge:Be	43. – 50.	1
	SW2-SW5, LW1	Ge:Ga	50 to 110 (10)	five 1
	LW2-LW5	Ge:Ga (stressed)	110 to 190 (20)	four 1

Table 1. List of the IR detectors on-board ISO with indications of type, operating wavelengths (peak or range) and detector topology (individual pixel, linear or matrix array).

1.1. Plan

Up to now, the efforts have been essentially focused on Si:Ga and Ge:Ga detectors. In Sect. 2, we present our works on transients for the Si:Ga detectors. We describe a non linear model used for uniform illumination in Sect. 2.2. Because of the peculiarities of transients for point source, a simplified tri-dimensional (3D) model is proposed in Sect. 2.3. Finally, we discuss in Sect. 2.4 the remaining problems. In Sect. 3 it is shown that, at the present time, the transient effects of Ge:Ga detectors are not qualitatively described by a model coming from physics. Therefore we present an empirical model for PHT C-100. A brief overview on the status for the other detectors on-board ISO is done in Sect. 4.

The transient correction requests both a good model and an efficient inversion method. In Sect. 5, we propose several methods used on ISO data to correct the transients. In Sect. 6 we discuss other dedicated data processing techniques connected to the transient effects. In Sect. 7 we summarize what we have learned on transients from ISO.

1.2. Some definitions

Let n be the index of the sky position of the satellite and t the time at the end of each integration. Elementary measurements of the detector at the end of each integration time are readouts $J_n(t)$. Generally, each readout is computed from the curve which gives the evolution of the number of charges as a function of the integration time (the "ramps", containing non destructive measurements between resets). This operation may be not trivial because of non linearities of the electronics and glitches due to high energetic particles. In the case of PHT[30] and LWS,[31] the ramps are adjusted with a low order polynomial. For CAM, only 2 points are measured due to telemetry limitations. Systematic errors coming from this step are not considered here.

Because of memory effects, each position n on the sky is observed during several readouts; this set of readouts gives the block n. Let us note t_n, the instant of flux changes and J_n^∞ the value of the readouts when the stabilization is achieved over the n-th block. This current J_n^∞ is proportional[22] to the constant incoming flux observed during this n-th block. Corresponding readouts are denoted $J_n(t)$ for $t \in [t_n, t_{n+1}[$.

2. SI:GA DETECTORS

2.1. The Si:Ga detectors on-board ISO

Several detectors are in Si:Ga on-board ISO (Table 1) : the LW 32×32 matrix array of the CAM[7,8] camera, three detectors of the PHT[32] photometer (S1, S2 and P) and one 1×12 linear array of the SWS[14] short wavelength spectrometer (band 2). Before the launch of ISO, ground based tests were extensively performed (CAM,[34] PHT[25,37,35] and SWS[45]). No accurate model for transients was developed for SWS and CAM. A promising non linear model was optimized[22] for PHT-S, while several problems occurred due to temperature variations due to the Cold Readout Electronic (CRE) and CRE CMOS transistors latch-up.[30] The initial model was also modified in order to include temperature variations correction.[22,37]

2.2. Uniform illumination case : the Fouks model

During ground based tests and the ISO mission the transients were studied and several linear and non-linear models have been suggested. As we explain below with the CAM-LW example, it became evident that the models must be non linear and must take into account the history of the illumination of the pixels.

Under quasi uniform illumination (low gradient of illumination on the pixel surface and between adjacent pixels), the transients of CAM-LW matrix array have several properties[34,1,13] :

- an instantaneous jump of the current after a flux change, of ~50% of the new steady state current;
- a time constant inversely proportional to the incoming flux;
- the transients are non linear (see Fig. 9 in[34]);
- they are highly reproducible when the pre-history is the same;
- they strongly depend on the pre-history (see Fig. 6 in[13]);
- when $J^{\infty}_{n+1}/J^{\infty}_{n} > 2.$, the upward step is characterized by an inflection point, the position of this point is related to the ratio $J^{\infty}_{n+1}/J^{\infty}_{n}$;
- downward steps are hyperbolic-like.

As a consequence, the response should be described with a non linear and non symmetrical model. Such analytical models have been developed for IR detectors by Vinokurov and Fouks[43] from the non-linear equations[43,26] describing such detectors. One of these models, the so-called Fouks-Schubert model, was used for describing transients of PHT-S detector during ground based tests.[22,35–37] We indicate here the formula[22,13] when starting from an unstabilized current J^{end}_{n-1} at the end of block $n-1$:

$$J_n\left(t\right) = \beta J^{\infty}_n + \frac{\left(1-\beta\right) J^{\infty}_n \left(J^{end}_{n-1} - \beta J^{\infty}_{n-1}\right)}{\left(J^{end}_{n-1} - \beta J^{\infty}_{n-1}\right) + \left[\left(1-\beta\right) J^{\infty}_n - \left(J^{end}_{n-1} - \beta J^{\infty}_{n-1}\right)\right] exp\left(-J^{\infty}_n t/\lambda\right)}, \tag{1}$$

where the time t is measured from an arbitrary instant after the flux change at time $t=0$, β the instantaneous jump and λ a constant. The unstabilized current J^{end}_{n-1} before the flux change reflects the history of the detector (stabilization in block $n-1$ is achieved when $J^{end}_{n-1} = J^{\infty}_{n-1}$); J^{∞}_n is the steady-state current under the constant incoming flux during block n.

For a wide dynamical range, the comparison of this formula with experimental data for the CAM-LW detector has shown its high exactness. For 90% of the pixels, it is possible to adjust β and λ parameters to fit the transient response with an accuracy better than 5 % for each readout $J_n(t)$ during a block, then the accuracy on the computed value of J^{∞}_n is about a few %. The parameters (β,λ) for each pixel of the matrix array have been adjusted one time on a limited number of data sets; they were unchanged during the life of ISO in space (~28 months).[13] The comparison of J^{∞}_n with the steady-state calibration of the detectors allows us to derive the incident fluxes with a precision better than few %.

A modified version[29] of this Fouks model has been developed with success for the band 2 of SWS. Time variations of the dark current have to be included.

This simple non-linear analytical formula (Eq. 1), taking into account the memory effects, is directly derived from a set of conventional 1D physical equations. These equations describe the processes in the detector bulk, with the use of Fouks' boundary condition[18] that describes the properties of the detector contacts. This boundary condition has been used in the form :

$$p\left(0,t\right) = p\left(0,0\right) exp\left[\frac{\Delta E\left(0,t\right)}{E_j}\right] \tag{2}$$

where $p\left(z,t\right)$ is the hole concentration at the plane z measured from the injecting contact placed at the plane $z=0$, the time t is measured from an arbitrary instant, as in Eq. (1), $\Delta E\left(0,t\right)$ is the change of the near-contact field with time ($\Delta E(0,t) = E(0,t) - E(0,0)$), E_j is the characteristic of the injection ability of the contact. Eq. (2) permits to describe the contact properties with a high exactness[22] and, in addition, to include into consideration the additional technological and engineering effects being inherent to the really created detectors.[23]

The use of Eq. (2) instead of consideration of the processes inside the near-contact space-charge region highly simplifies the description of transient currents. Nevertheless, in general it remains rather complex even after this simplification. However, in the case where E_j is much less than the steady-state field in the detector bulk, $E_0 = V_0/l$ (where V_0 is the steady-state voltage applied to the detector, l is the inter-contact distance), this description can be additionally strongly simplified, and Eq. (1) serves as a very exact description for transient currents.[43] The parameter E_j quantifies the quality of the contacts and depends on the flatness of the donor profile in the near-contact region and is linked to the time constant of the current relaxation. The higher the contact quality, the less is E_j, and the shorter the time constant. In real detectors under helium temperatures E_j is of order of 10^2-10^3 V/m. For Si:Ga detectors E_0 is typically 10^5-10^6 V/m, that provides very high exactness of Eq. (1). In Ge:Ga detectors E_0 is of order of E_j that makes this formula inexact.

The other important point lies in the fact that Eq. (1) is applicable only in the case where the illumination is uniform on the pixel surface. In this case high photoelectric non-stationary crosstalkings between adjacent pixels, that are inherent to such detectors,[22] compensate each other that makes the electric field being uniform along the planes z and the used 1D equations being true. Under non-uniform illumination the set of 1D equation can't be used, and Eq. (1) looses its exactness.[42,44]

2.3. Cross-talk : the problem with point sources

Eq. (1) reproduces the experimental data only under homogeneous irradiation of the array. The transients for point-sources are different. This is due to 3D effects inside the array. These effects are caused by the fact that the screening length for the charges, created in the bulk of low-background detectors under a time-variable irradiation, is very long. As a result, the field of the charges penetrates through the bulk and spreads to all sides creating 3D picture of the force lines of the field.[42,21,44] However, under homogeneous irradiation, the influence of the 3D field effects on the transient current in the detector can be described with a good exactness in one dimensional (1D) approximation with the use of the field averaged along the contact planes and with the re-normalization of the contact parameter[23] E_j. For highly inhomogeneous irradiation such approach is impossible, and 3D equations must be used. They are :

$$\text{the continuity equation} \;:\quad \nabla(p\mathbf{v}) = -\frac{p(\mathbf{r},t)}{\tau} + G\left(\mathbf{r},t\right), \tag{3}$$

$$\text{the Poisson equation} \;:\quad \nabla\mathbf{E} = \frac{4\pi e}{\kappa}\rho\left(\mathbf{r},t\right), \tag{4}$$

$$\text{and the trap recharging equation written in the form} \;:\quad \frac{\partial\rho\left(\mathbf{r},t\right)}{\partial t} = \frac{p\left(\mathbf{r},t\right)}{\tau} - G\left(\mathbf{r},t\right). \tag{5}$$

Here $p\left(\mathbf{r},t\right)$ is the hole concentration, τ the capture time, $\mathbf{v}\left(\mathbf{r},t\right)$ the drift velocity of the holes, $G\left(\mathbf{r},t\right)$ the generation rate, $\rho\left(\mathbf{r},t\right)$ the density of the charge accumulated in the traps. In principle, these equations have to be supplemented by the boundary conditions describing the equipotentiality of the contacts and the absence of the current through the free surfaces of detectors. Below we'll consider the simplified plane geometry case. We suppose that the detectors represent continuous photoconductive media confined by two contact planes (at $z = 0$ and $z = l$) with fixed potentials (0 and V_0). This provides the steady-state field $E_0 = V_0/l$ directed along the z-axis. The following consideration is carried out under the condition :

$$E_0 \gg E_j \tag{6}$$

which is always true for usual Si:Ga detectors. This permits to ignore the effect of non-stationary fields on the drift velocity and rewrite Eq. (3) as :

$$v\frac{\partial p\left(\boldsymbol{\rho},z,t\right)}{\partial t} = -\frac{p\left(\boldsymbol{\rho},z,t\right)}{\tau} + G\left(\boldsymbol{\rho},z,t\right), \tag{7}$$

where $v = \mu E_0$ and $\boldsymbol{\rho}$ is the transverse coordinate. Next we suppose that the generation is independent on the coordinate z : $G\left(\boldsymbol{\rho},z,t\right) = G\left(\boldsymbol{\rho},t\right)$. In this case the solution of Eq. (7) has the form :

$$p(\boldsymbol{\rho}, z, t) = p(\boldsymbol{\rho}, 0, t)\, e^{-\frac{z}{\tau v}} + \tau G(\boldsymbol{\rho}, t)\left(1 - e^{-\frac{z}{\tau v}}\right). \quad (8)$$

The substitution of this formula for the hole concentration in Eq. (5) gives the expression for the time derivative of the charge density :

$$\frac{\partial \rho(\boldsymbol{\rho}, z, t)}{\partial z} = \left[\frac{p(\boldsymbol{\rho}, 0, t)}{\tau} - G(\boldsymbol{\rho}, t)\right] e^{-\frac{z}{\tau v}}. \quad (9)$$

From Eq. (4) we can deduce the equation that links the z-field component at the contact plane $z = 0$ with the charge density in the detector bulk :

$$\frac{\partial E_z(\boldsymbol{\rho}, 0, t)}{\partial t} = \int d\boldsymbol{\rho}_0 \int_0^l dz_0 E_z(\boldsymbol{\rho}, 0, \boldsymbol{\rho}_0, z_0)\, \frac{\partial \rho(\boldsymbol{\rho}_0, z_0, t)}{\partial t}, \quad (10)$$

where the Green function of the Poisson equation for the used plane geometry is defined by the expression taking into account the effect of image charges :

$$E_z(\boldsymbol{\rho}, 0, \boldsymbol{\rho}_0, z_0) = -\frac{2e}{\kappa} \sum_{n=-\infty}^{n=\infty} \frac{(2n-1)\, l + z_0}{\left(\left[(2n-1)\, l + z_0\right]^2 + (\boldsymbol{\rho} - \boldsymbol{\rho}_0)^2\right)^{3/2}}. \quad (11)$$

Now using the boundary condition, which has the next form for the 3D case :

$$p(\boldsymbol{\rho}, 0, t) = p(\boldsymbol{\rho}, 0, 0)\, exp\left[\frac{\Delta E_z(\boldsymbol{\rho}, 0, t)}{E_j}\right] \quad (12)$$

(here $\Delta E_z(\boldsymbol{\rho}, 0, t)$ is the non-stationary z-component of the field in the contact plane) and, from Eqs. (9) and (10), one obtains the integral-differential equation for this field component :

$$\frac{\partial E_z(\boldsymbol{\rho}, 0, t)}{\partial t} = \int d\boldsymbol{\rho}_0 K(\boldsymbol{\rho} - \boldsymbol{\rho}_0)\left[G(\boldsymbol{\rho}_0, t) - \frac{p(\boldsymbol{\rho}, 0, 0)}{\tau}\right] exp\left[\frac{\Delta E(\boldsymbol{\rho}_0, 0, t)}{E_j}\right] \quad (13)$$

with the kernel described by the expression :

$$K(\boldsymbol{\rho}) = \frac{2e}{\kappa} \int_0^l dz \sum_{n=-\infty}^{n=\infty} \frac{2nl + z}{\left[(2nl + z)^2 + \boldsymbol{\rho}^2\right]^{3/2}} e^{-\frac{z}{\tau v}}. \quad (14)$$

Under homogeneous irradiation, $G(\boldsymbol{\rho}, t) = G(t)$, one can deduce from Eqs. (13) and (14) the following equation :

$$\frac{\partial E_z(0, t)}{\partial t} = \frac{4\pi\beta}{\kappa}\left[e\tau v G(t) - evp(0, 0)\, exp\left[\frac{\Delta E(0, t)}{E_j}\right]\right], \quad (15)$$

where $\beta = 1 - g\left(1 - e^{-1/g}\right)$ and $g = \tau v / l$. This equation permits to deduce analytically Eq. (1) for uniform illumination.[22] Under inhomogeneous irradiation Eq. (14) (with Eq. (15)) has to be solved by computations. The computed field distribution along the contact plane, separated into individual squared detector areas of side a with the centers $x = na$ and $y = ma$, where n and m are the whole numbers, permits to find the currents through these detectors :

$$J_{n,m} = \int_{S_{n,m}} d\boldsymbol{\rho}\left[evp(\boldsymbol{\rho}, 0, 0)\, exp\left[\frac{\Delta E(\boldsymbol{\rho}, 0, t)}{E_j}\right] + \frac{\kappa}{4\pi} \frac{\partial E_z(\boldsymbol{\rho}, 0, t)}{\partial t}\right], \quad (16)$$

where the areas $S_{n,m}$ are restricted by the conditions : $na - \frac{a}{2} \leq x \leq na + \frac{a}{2}$, $ma - \frac{a}{2} \leq y \leq ma + \frac{a}{2}$. The computational results for different inhomogeneous fluxes and different pixels are presented in Fig. 1.

2.4. The new status on transients for Si:Ga detectors

At the present time, the Fouks 1D non-linear model is a clear improvement for describing transients of the Si:Ga detectors of CAM, PHT and SWS. Several problems which were not seen or were misunderstood before its use became clear after correction with this model because they give evident deviations from this model.

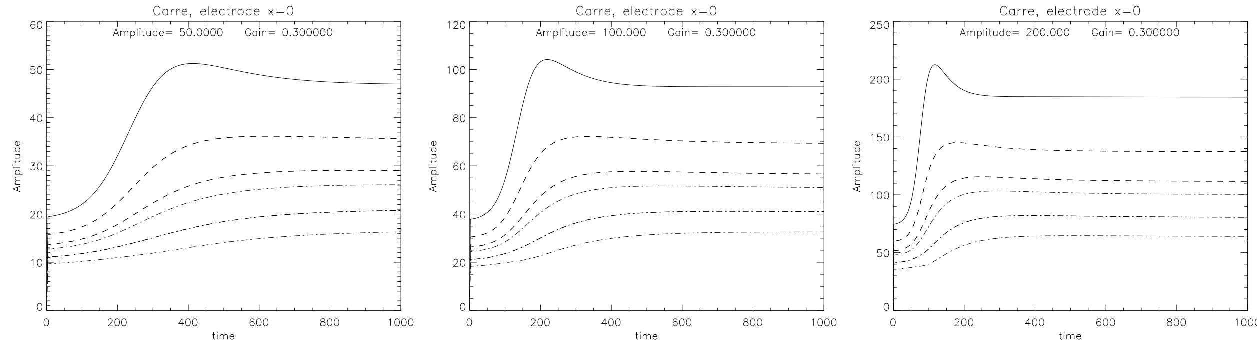

Figure 1. Three transient responses for the same point spread function profile with three different amplitudes. The source is off-centered by (1/4,1/4) of pixel size. The continuous line shows the transient response for the central pixel, the dashed lines are for the the 4 adjacent pixels (only 2 lines because of symmetry) and the dot-dashed lines are for the diagonal pixels (3 lines). The computed results illustrate the current spreading (the appearance of the current in dark regions neighboring to the illuminated ones) that results from the spreading of field lines and the current overshooting that results from a high current density in the region under a high-density flux. The presented results give rather good qualitative description of the transients under point-source illumination. In order to receive an exact quantitative description of the transients the theory has to take into account the real topology of the detectors and their conductive surroundings.

For CAM-LW, observed deviations are the Long Term Drift (LTD),[13,33] the Small Amplitude damped Oscillations (SAO) and the specific transients for point sources (Sect. 2.3). Several models for LTD and SAO were suggested,[43,23] but ground based tests and in-flight observations were not convenient to test these models with enough accuracy (see Sects. 6 and 7).

For SWS, electrical glitches and saturation above a given level became the new limiting factors. As below this saturation level the Fouks 1D model is good enough to describe any flux change, it is under investigation that this saturation is coming from cross-talk between pixels, change of the illumination profile on the detector surface (point source problem) or is a true saturation problem.

For PHT-S and PHT-P1, even (1) if a good agreement was achieved between transients and Fouks models during ground based tests and (2) if transients shapes did not change significantly during flight, use of this model on in flight data was unsuccessful. Several facts could explain that change in the behavior of the detectors.

High energetic particles which hit the detector generate electron-hole pairs that results in visible glitches and in accumulation of invisible positive (hole) and negative (electron) charges captured in the bulk. These charges have to modify the parameters and operation of the detector.[37] The used electrical curing could not completely restore the parameters and the detetector operation. CAM-LW has an other design[3,7] : the upper side is set to $\sim$25 V, the lower side, connected through Indium bumps to CRE, is the reference (0 V) and the reflecting plane added around the contacts at lower side is set to $\sim$5 V. Undesirable charges in the detector are likely evacuated through this channel. Furthermore, in order to avoid changes of the parameters, the CAM-LW detector was never electrically switch off.[17]

In summary, for uniform illuminated Si:Ga detector, very good results have been obtained with the Fouks model as a first order model since the accuracy was $\sim$10 % with previous models[1] and $\sim$1 % with this one.[13] Then other effects as small oscillations, long term drift, cross-talk, change of the parameter at the sides of matrix detector, become the main problems to be resolved. Since the Fouks model comes from physics, it gives way to improve future Si:Ga detectors.

During the study of such non linear model, it became evident that the raw data must be well pre-processed. Especially the subtraction of the dark level must be as precise as possible. For CAM-LW[5] and SWS,[29] the dark correction has to include temporal variations.

3. GE:GA DETECTORS

3.1. The Ge:Ga detectors on-board ISO

Several Ge:Ga detectors have been set up for the ISO satellite (Table 1) : one detector and two small matrix array for PHT[32,46] (P3, C-100 3×3 pixels, stressed C-200 2×2 pixels), and several stressed (4) and un-stressed (5) monolithic detectors for LWS.[12,9,46] All of these are affected by transient effects which can bias the final photometry typically from 10 to 40 %. Some of them present a hook response (quick overshoot) for high upward steps of flux. However, these transients appear much more easy to modelized than Si:Ga ones because they are at a first order exponential[9,12] and have no inflection point. Then the need of non linear models seems to be less sensitive in order to take into account the memory effect.

At the present time, outside ISO teams, the two main ways to study the Ge:Ga detector transients were the works done by the N. Haegel team[26] and by the Fouks team.[19] The N. Haegel team has developed numerical codes in order to solve the set of non-linear differential equations constrained by some boundaries conditions. After improving their code in order to be able to compute transients for thicker bulks and for low levels, they are working now on the problem of transients under non uniform illumination. The Fouks team solved their general model, in first turn, by analytical methods. This highly simplifies the solutions, alleviates the comprehension of the physics of the observed phenomena, permits not only to consider the behavior of an ideal detector, but also to include into the consideration a lot of additional essential phenomena appeared under effect of the real technology and design peculiarities of the detectors. However, following Fouks classification[43,19] based on the ratio E_0/E_j (see Sect. 2.2) for Ge:Ga detectors we are unfortunately always in a defavourable domain and the expected accuracy of such simplified analytical models, even if the detector is perfect, is about 10-20 %. Fouks team also has made computative descriptions for some transient curves for Ge:Ga detectors.[19] However, up to now none of these two approaches have been applied on data to correct the Ge:Ga transients.

3.2. Status on transient correction

The present status on transients for the Ge:Ga detectors is much less favorable than for Si:Ga detectors :

- each Ge:Ga detector seems to require a peculiar model,
- several fitting methods are available in the PIA software used for interactive analysis of the PHT data,[24] but no peculiar models is definitively affected for each Ge:Ga detector;
- a empirical model based on a Fouks one have been developed for several bands of LWS, with a clear improvement on the shape of the spectral lines.[6] In all cases, non linear models have to be used to reproduce properly the memory effects.

At that time, several conclusions are coming :

- no universal model like Fouks model for Si:Ga has been pointed out,
- the linear models based on fitting 2 or 3 exponentials did not work on a wide dynamical range for these detectors,[10,11]
- empirical non-linear models give interesting but not definitive results, at the price of huge works,
- the use of an extended calibration database is in any case essential to build realistic models of the transient response.

3.3. One peculiar case : transient of Ge:Ga PHT C-100

A preliminary study[38] has been devoted to PHT C-100 transients. After testing different models (linear and non linear, empirical or physical from Fouks' team[19]), we have concluded that only an empirical non linear model with a non symmetrical behavior can simply reproduce the observations :

- downward incoming flux step results in an instantaneous decrease of $J_n(t)$ down to J_n^∞
- upward incoming flux step results, after an instantaneous jump β in an exponential increase of $J_n(t)$ up to J_n^∞.

Moreover, the memory effect from the block $n-1$ into the n-th one is taken into account (in an approximated form) and, as seen in the data, the memory effect is reseted when a downward step occurs.

Direct model then reads :

$$\text{for } t \in [t_n, t_{n+1}[\quad J_n(t) = \begin{cases} J_n^\infty & \text{if } J_n^\infty < J_{n-1}^\infty \\ J_n^\infty - (1-\beta)(J_n^\infty - J_{n-1}^\infty)\exp(-J_n^\infty(t-t_n)/\lambda) & \text{if } J_n^\infty > J_{n-1}^\infty \end{cases} \tag{17}$$

(with same notations than in Eq. (1)) which can be rewritten in a unique expression :

$$J_n(t) = J_n^\infty - (1-\beta)\varphi(J_n^\infty - J_{n-1}^\infty)\exp(-J_n^\infty(t-t_n)/\lambda), \quad t \in [t_n, t_{n+1}[\tag{18}$$

with $\varphi(u) = 0$ if $u \le 0$ and $\varphi(u) = u$ if $u > 0$. The dedicated inversion method is described in Sect. 5.

4. OTHER DETECTORS

Concerning SWS, band 1 (In:Sb) and band 3 (Si:As BIBIB) are completely free of transient effects,[29] but the band 4 (Ge:Be) and the 2 Fabry-Pérot bands (Si:Sb and Ge:Be) are affected.[45,29] Up to now, no efficient model has been found for the band 4. The consequences of transients on the Fabry-Pérot bands (FP in Table 1) appear at the present time limited. The SW CAM CID In:Sb 32×32 matrix array is affected by a transient effect without instantaneous jump ($\beta = 0$). Empirical model has been developed.[41] Following ground based experiments, PHT P2 (Si:B) is affected by very limited transients. The SW1 channel for LWS (Ge:Be) is affected by transients,[10] and no model is used at that time. Several of these detectors are still under study for transient correction.

5. CORRECTION METHODS : AN INVERSE PROBLEM

The present Section is devoted to transient correction tackled as an *inverse problem*. Subsection 5.1 describes some elements of the proposed framework while Subsection 5.2 develops such an approach in order to correct transient effects of PHT model described in Sect. 3.

5.1. Inverse problems

Inverse problems play an important role in numerous branches of engineering and applied physics : medical imaging, geophysics, astrophysics, *etc,* ... . In such fields, objects of interest (denoted $x \in \mathbb{R}^N$) can only be observed through measurement system (denoted H). Such a system often involves blurring effects, transient response, high frequencies cut-off, *etc,* ... . Hence, the experimentalist, must start with an observed data set (denoted $y \in \mathbb{R}^P$), which is a degraded version of the true object x. In our context, measurements *i.e.* readouts $J_n(p)$, $p = 1, \ldots, P$ are a degraded version of the stabilized values J_n^∞, $n = 1, \ldots, N$. This degradation is essentially due to transient effects. Computations are then needed in order to *inverse* the distortion of the measurement system. Such a problem is usually decomposed in two sub-problems.

1. A *direct problem* founded on physical equations. Given the *true* object x and the physical properties of the observation system, one mathematically describes experimental readouts y. Such a model usually reads $y = H(x) + b$, where b accounts for model and measurement errors. The model H must be accurate enough in order to account for detailed physical phenomena at work and simple enough in order to allow efficient computations.
2. An *inverse problem* founded on data processing methods. Given the observed data set y and the physical model H, one inverses the data flow and decodes the true object from the observed data. In other words, the aim is to build an estimation $\hat{x}$ of the object x on the basis of the data set y and using the model H.

In spite their apparent diversity, most of the inverse problems encountered in applied physics suffer from a common feature[15,27] : *ill-posedness*, especially if $P < N$ or $P \simeq N$. Roughly speaking, this is due to the degradation achieved by observation systems : they definitely "corrupts" information from the true object into the data. So, information is missing in order to robustly inverse the system. Under such circumstances, reconstruction of the sought object x becomes tricky or even impossible on the sole basis of the data : small errors in the observed data may result in large errors in the reconstructed objects.

Numerous methods have been proposed to cope with ill-posedness (see[15] and references therein). In order to construct a reliable object, structural information is needed concerning the sought object. Solutions are brought by restricting the class of admissible solutions given suitable informations. A widely used and powerful framework for this task is the *regularization* one. This tool accounts for foreknown informations about the sought objects, in order to compensate, at least partially, the lack of information provided by the data.

5.1.1. Accounting for model and data

Observed data y and mathematical model H are taken into account by means of a measure of discrepancy between observed data y and model output $H(x)$. The most simple choice for this measure is a quadratic distance, *i.e.* a Least Square (LS) criterion[39] :

$$Q_{\mathrm{LS}}(x) = \| \, y - H(x) \, \|^2 \, . \tag{19}$$

The usual fitting procedure, often used in experimental data processing, yields the LS estimate :

$$\hat{x}_{\mathrm{LS}} = \arg\min_x Q_{\mathrm{LS}}(x) \, . \tag{20}$$

5.1.2. Accounting for prior information

As mentioned above, a commonly used way of dealing with ill-posedness is the regularization framework which consists in accounting for available prior information. This can be achieved by means of at least three strategies : *penalization*, *constraint* or *re-parameterization*. Moreover, a combination of these strategies is clearly possible if needed.

Penalization — A penalized form yields a regularized least squares criterion :

$$Q_{\mathrm{RLS}}(x) = Q_{\mathrm{LS}}(x) + \alpha\,\varphi(x) \tag{21}$$

where $\varphi(x)$ measures a discrepancy to a prior information. Such a criterion strikes a compromise between information provided by the data and prior information. The hyperparameter, namely α, controls the trade off between the two sources of information.

Constraint — A constrained approach yields another class of optimization problem :

$$\min_x Q_{\mathrm{LS}}(x) \qquad \text{s.t.} \quad x \in \mathcal{D}\,, \tag{22}$$

that is a constrained optimization problem (s.t. stands for "subject to"). The set $\mathcal{D}$ must be specified according to the context. For example, if the sought object is a light flux or an energy, hence positive, a natural choice reads $\mathcal{D} = \mathbb{R}_+^P$.

Re-parameterization — Information can also be accounted for by means of a new parameterization, such as $x = x(\theta)$ of the sought object. Parameter θ can then be estimated in a LS framework.

5.1.3. Optimization stage

The key property in numerous optimization problem is *convexity*.[4] Under such assumption a unique global minimum exists for the previously proposed criterion. Moreover, the global minimizer can be reached by means of classical optimization methods such as gradient or coordinatewise descent algorithm. Unfortunately, the model at work in our context is a non-linear one and convexity property will not be ensured. As a consequence, no guarantee of global minimization will be provided.

5.2. Block by block inversion method

Sect. 3.3, Eq. (18) describes an empirical model for PHT C-100 detectors. The present Section is devoted to correction of transient effects within the proposed framework. Two kinds of information are available :

1. the sought incoming flux is positive and
2. "by construction" a piecewise constant signal.

The idea developed here is to account for these informations in order to robustify inversion. This kind of prior knowledge can be captured mathematically and exploited in a constrained framework shortly described above. Given the direct model of Eq. (18), the LS criterion reads :

$$Q_{\mathrm{LS}}(J^\infty) = \sum_{n=0}^{N-1}\sum_{p=0}^{P-1}\left[J_n(p) - \left(J_n^\infty - (1-\beta)\varphi(J_n^\infty - J_{n-1}^\infty)\exp(-J_n^\infty(p-p_n)/\tilde{\lambda})\right)\right]^2 \tag{23}$$

with $\tilde{\lambda} = \lambda F_s$ (F_s is the sampling frequency). Index n runs over the block indices and p runs over the readouts indices. Due to the specificity of the memory effect, each term of the first sum only depends on two values of the stabilized values, so Q_{LS} can be rewritten :

$$Q_{\mathrm{LS}}(J^\infty) = \sum_{n=0}^{N-1} Q_n(J_n^\infty\,,\, J_{n-1}^\infty). \tag{24}$$

As mentioned above, the property of the direct model does not allow us to ensure global minimization of (24) over $\mathbb{R}_+^N$. But, taking advantage of the specificity of the criterion, global minimization is possible over a finite subset of $\mathbb{R}_+^N$: an arbitrary fine regular grid of K possible values of the stabilized value : $G_J = \{J_{\max}k/K\}_{k=0,\ldots,K-1}$.

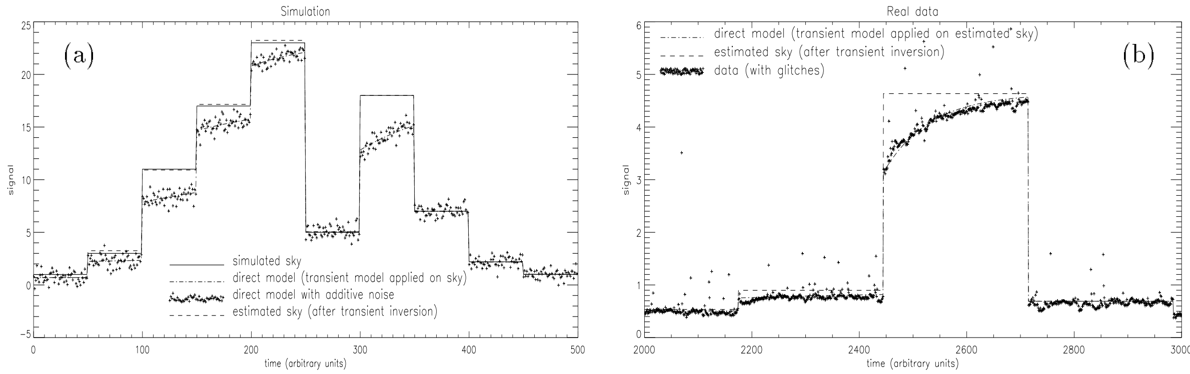

Figure 2. Data processing according to the proposed approach. Fig. (a) illustrates simulated data processing while (b) results from real data processing in the presence of glitches, which give a limited overestimated value for the step. For real data, the interblocks data -when the satellite pointing direction is changing- are removed before processing. This is a simplification. In the future, these interblocks will have to be included in the processing to improve the accuracy of the correction.

A dynamic programming algorithm has been implemented in order to achieve minimization over G_J. The idea is simple : compute the values of $Q_N(J^\infty_{N-1}, J^\infty_N)$ for the K^2 possibles values of $J^\infty_{N-1}, J^\infty_N$. The minimizer with respect to J^∞_N is then available as a function of J^∞_{N-1}. The following steps consist in shifting indices by -1 and repeat the same operation with Q_{N-1}, Q_{N-2}, down to Q_0. The last step gives the minimizer with respect to J^∞_{-1}. Then a forward tracking step recursively gives the minimizer with respect to J^∞_{-1}, J^∞_0, ... J^∞_N. The procedures clearly reach the true minimum of criterion (23), over the defined grid G_J. Optimum can the be refined using a gradient procedure, not described here.

5.2.1. Computation results : simulated data

The first step of the proposed computation study relies on simulated data according to model of Eq. (18). "True" stabilized value J^∞_n, simulated data $J_n(p)$ and estimated stabilized values $\hat{J}^\infty_n$ are shown in Fig. 2-(a). It can be clearly stated that the proposed method properly inverse the system and correct transient : the reconstruction error between $\hat{J}^\infty_n$ and J^∞_n is less than 1%.

5.2.2. Computation results : real data

This part is devoted to real data analysis also presented in Fig. 2. According to Fig. 2-(b), the proposed method seems to process real data as well as simulated ones of Fig. 2-(a). However, as shown in Fig. 2-(b), the presence of glitches tends to slightly over estimate the stabilized value, as expected form a quadratic criterion in presence of positive "impulsive" noise. In the proposed framework, future works will be devoted to glitches modelization by means of Poissonian noise.

5.3. Readout by readout inversion methods

For CAM-LW, only readout by readout inversion methods have been implemented at that time.[1,13] Such methods work in two steps. First for each readout a stabilized value is computed. It is a special case of the block by block method with a block size of one. Second the stabilized values are averaged over each block. The block by block inversion method presents the advantage to take into account properly the piecewise constant character of the incoming flux which avoids the pitfalls of applying a two step procedure. In the block by block framework, the number of unknown parameters comes down from P to N *i.e.* is reduced by a factor M (if M readouts per block), with respect to a readout by readout methods. So, statistical properties improvement can be expected.[39]

6. SPATIAL AND TEMPORAL FILTERINGS; USE OF THE REDUNDANCY

In several observations, the main error for data processing under quasi uniform illumination did not come from transients but from glitches, Long Term Drift (LTD) or Small Amplitude damped Oscillations (SAO). Especially observations of very faint point sources or extended structures on top of uniform illumination (e.g. zodiacal emission) with CAM-LW can be contaminated by glitches, LTD and SAO.

When the scientific objective is to extract real faint point sources (e.g. cosmological surveys), LTD and SAO can be more or less easily removed using spatial or temporal filterings. In that case, the limiting factor is the glitches,[2,20] especially the strongest and the faintest ones. Methods based on wavelets[40] or temporal filtering[16] have been used to reject artefacts due to glitches.

On the contrary, when the scientific objective is to measure the emission of low contrasted extended structures (e.g. diffuse interstellar clouds) the limiting factors are LTD and SAO. Because different sky positions have been generally observed several times, a method based on the use of the redundancy can be applied.[33]

For SWS observation and for spectroscopic observations with the Circular Variable Filter of CAM-LW, the spectra are often observed with direct and reverse scanning direction. If the transient model and the transient correction are perfect, these direct and reverse scans after correction must be superimposed. This strong constrain can be used to estimate very accurately the initial conditions J_0^{∞}, which is generally unknown, in Eq. (1) for the transient correction. On the contrary, observations with only one scanning direction cannot be transient corrected without any ambiguity when they start at low level because of the very long memory effect at such low levels.

7. CONCLUSION : WHAT WE HAVE LEARNED FROM ISO

Several important facts about transients of low background IR detectors have been learned during the ISO mission. Furthermore, dedicated signal processing methods have been set up for correcting these transients.

One very important result, true for all the Ge:Ga and Si:Ga detectors which have been analyzed is that all of them present reproducible memory effects and non linear transient behavior. The models to describe such transients must be non linear and the data pre-processing (dark correction) must be as accurate as possible since the response depends on the value of the measured signal above the dark level. This problem is obviously more critical at low level.

For most of the Si:Ga detectors on-board ISO under quasi uniform illumination, a 1D non linear model based on physics describes with a precision of a few % the transient responses observed during the flight. Other effects (Long Term Drift, Small Amplitude Oscillations, limited hook effect at very high flux steps, ...) have been predicted before ISO mission[42] and have been observed in SWS, PHT and CAM transients. Unfortunately, due to time constrains during the ISO life, a limited number of tests were performed to characterize these second order effects. Moreover the data sets are often perturbated by parasitic effects (time discontinuity for CAM ground based data, glitches during flight, ...). In any case, the experience from ISO will be very useful to optimize future generation of Si:Ga detectors used in astronomy.

Another result concerns the electrical cross-talk between pixels in linear and matrix arrays which can be very strong. Unfortunately, point source measurements are often not optimal (too short observations, unproper initial conditions, limited number of configurations) in order to characterize accurately the cross-talk during the flight. For Si:Ga matrix array, promising qualitative results have been achieved with the simplified 3D model described in Sect. 2.3. We are currently working on a more complicated one.

Following Fouks theory of such detectors, it is predicted that the behavior of Ge:Ga detectors is much more difficult to describe using analytical models from physics (less simplification in non-linear differential equations and more technical difficulties to make such detectors ...). Nevertheless it may be possible to describe the transients in Ge:Ga detectors with acceptable exactness by computations based on Fouks general model, but this work is complex and it could be complicated by extra physical (quantum) effects inherent to Ge:Ga detectors and especially the stressed ones. The next generation of Ge:Ga matrix arrays for SIRTF and ASTRO-F may also present complicated transient effects. For these future detectors, ground based tests using what we have learned form ISO have to be systematically performed in order to prepare transient corrections.

ACKNOWLEDGMENTS

AC thanks CNES, CEA SaP and IAS for financial support. AC is debtfull with B. Fouks, him incredible knowledge of the physics of such low background IR detectors, him kindness and pedagogy. We thank L. Vigroux, A. Agnèse and P. Mottier, designers of CAM-LW, E. Caux (LWS), P. Garcia-Lario, D. Kester (SWS), B. Schulz (PHT) and all the other members of the ESA Transient Working Group for their helps (please contact P G-L (`pgarcia@iso.vilspa.esa.es`) for any informations concerning this WG). Several informations of this work are coming from ESA Transient Work Group (`http://www.iso.vilspa.esa.es/`). We also thank M.-A. Mivile-Deschênes, K. Okumura, S. Bouaissi and F. Balleux.

REFERENCES

1. A. Abergel, M. A. Miville-Deschêne, F.-X. Désert, M. Pérault, H. Aussel, and M. Sauvage. IAS model for ISOCAM LW transient correction. *accepted in Experimental Astronomy*, February 1999.
2. P. Agnèse, J. J. Engelmann, and P. Mottier. Results of radiation tests performed on the ISOCAM infrared detector array. *IEEE Trans. on Nuclear Science*, 38:953–963, August 1991.
3. P. Agnèse, C. Lucas, P. Maillart, P. L. Mottier, Y. Lepennec, and P. Masse. The ISOCAM camera long-wavelength channel detector. *Proceedings of SPIE*, 1070:124–128, July 1989.
4. D.P. Bertsekas. *Nonlinear programming.* Athena Scientific, Belmont, Massachussetts, 1995.
5. A. Biviano et al. The ISOCAM dark current calibration report. Technical report, ISOCAM, November 1998.
6. E. Caux. Application of Fouks-Schubert transient correction method to LWS data: status and plans. Technical report, CESR, CNRS, France, 1999.
7. C. J. Cesarsky et al. Camera of the Infrared Space Observatory. *Optical Engineering*, 33:751–761, March 1994.
8. C. J. Cesarsky et al. ISOCAM in flight. *Astron. Astrophys.*, 315:L32–L37, November 1996.
9. S. E. Church, M. J. Griffin, M. C. Price, P. A. Ade, R. J. Emery, and B. M. Swinyard. Performance characteristics of doped-Ge photoconductors for the Infrared Space Observatory Long Wavelength Spectrometer. *Proceedings of SPIE*, 1946:116–125, October 1993.
10. S. E. Church, M. C. Price, M. J. Griffin, P. A. R. Ade, R. J. Emery, and B. M. Swinyard. Non-linear effects in doped-germanium photoconductors for the ISO Long Wavelength Spectrometer. In *ESA SP-356 Photon Detectors for Space Instrumentation*, pages 261–264, December 1992.
11. S. E. Church, M. C. Price, N. M. Haegel, M. J. Griffin, and P. A. R. Ade. Transient response in doped germanium photoconductors under very low background operation. *Applied Optics*, 35:1597–1604, 1996.
12. P. E. Clegg et al. The ISO Long-Wavelength Spectrometer. *Astron. Astrophys. Suppl. Ser.*, 315:L38–L42, November 1996.
13. A. Coulais and A. Abergel. Transient correction of the LW-ISOCAM data for low contrasted illumination. *Astron. Astrophys. Suppl. Ser.*, 141, February 2000.
14. T. de Graauw et al. Observing with the ISO Short-Wavelength Spectrometer. *Astron. Astrophys. Suppl. Ser.*, 315:L49–L54, November 1996.
15. G. Demoment. Image reconstruction and restoration: Overview of common estimation structure and problems. *IEEE Trans. Acoust. Speech, Signal Processing*, ASSP-37:2024–2036, December 1989.
16. F.-X. Désert et al. A classical approach to faint extragalactic source extraction from ISOCAM deep surveys. Application to the Hubble Deep Field. *Astron. Astrophys. Suppl. Ser.*, 342:363–377, February 1999.
17. ESA. *ISO Handbook Volume III (CAM), Version 1.0*, July 1999.
18. B. I. Fouks. Injection properties of contacts to high-resistivity semiconductors. I–II. *Sov. Phys. Semicond.*, 15(9):974–980, 980–986, September 1981.
19. B. I. Fouks. Nonstationary behaviour of low background photon detectors. In *ESA SP-356 Photon Detectors for Space Instrumentation*, pages 167–174, December 1992.
20. B. I. Fouks. Phenomena in low-background IR detectors under high-energy particles. *Proceedings of SPIE*, 2817:160–171, October 1996.
21. B. I. Fouks, V. F. Kocherov, I. I. Taubkin, L. A. Vinokurov, and N. B. Zaletaev. Photoresponse of low-background extrinsic infrared detector arrays. *Optical Engineering*, 33:1485–1491, May 1994.
22. B. I. Fouks and J. Schubert. Precise theoretical description of photoresponse for detectors of ISOPHOT's Si:Ga array. *Proceedings of SPIE*, 2475:487–498, June 1995.
23. B.I. Fouks. Theory of photoresponse of low-background IR detectors. *Proceedings of SPIE*, 3122:441–452, October 1997.
24. C. Gabriel and J. A. Acosta-Pulido. The ISOPHOT interactive analysis (pia). *The Universe as Seen by ISO. Eds. P. Cox & M. F. Kessler. ESA-SP 427.*, 427:73–76, March 1999.
25. U. Groezinger, S. Kirches, D. Lemke, J. Schubert, B. Schulz, and J. Wolf. Characterization of detectors and calibration of the ISOPHOT experiment. In *ESA SP-356 Photon Detectors for Space Instrumentation*, pages 329–333, December 1992.
26. N. M. Haegel, J. C. Simoes, A. M. White, and J. W. Beeman. Transient behavior of infrared photoconductors: application of a numerical model. *Applied Optics*, 38(10):1910–1919, April 1999.

27. J. Idier. Regularization tools and models for image and signal reconstruction (Invited Paper). In *3nd Intern. Conf. Inverse Problems in Engng.*, pages 1–6, Port Ludlow, U.S.A., June 1999.
28. M. F. Kessler et al. The Infrared Space Observatory (ISO) mission. *Astron. Astrophys.*, 315:L27–L31, November 1996.
29. D. Kester. The impact of memory effects correction on SWS data. Technical report, SRON, Netherlands, 1999.
30. R.J. Laureijs, U. Klass, P.J. Richards, and B. Schulz. *ISOPHOT Data Users Manual, V 4.1.* ESA, October 1999.
31. S. J. Leeks, B. M. Swinyard, T. Lim, and P. E. Clegg. Aspects of LWS processing. *The Universe as Seen by ISO. Eds. P. Cox & M. F. Kessler. ESA-SP 427.*, 427:81–84, March 1999.
32. D. Lemke et al. ISOPHOT - capabilities and performance. *Astron. Astrophys. Suppl. Ser.*, 315:L64–L70, November 1996.
33. M.-A. Miville-Deschênes, F. Boulanger, A. Abergel, and J.-P. Bernard. Original data processing for ISOCAM raster imaging of extended emission. accepted in A&A, 2000.
34. M. Pérault, F.-X. Désert, A. Abergel, F. Boulanger, Ch. Dupraz, A. Soufflot, C.J. Cesarsky, and L.G. Vigroux. Infrared Space Observatory camera calibration facility and preflight characterization. *Optical Engineering*, 33:762–770, March 1994.
35. J. Schubert. *Die Eichung des Infrarot-Gitterspektrometers im Satelliten-Experiment ISOPHOT und die Korrektur der Transienten seiner Detektoren.* PhD thesis, Max Planck-Institut für Astronomie, Heidelberg, 1995.
36. J. Schubert, B. I. Fouks, D. Lemke, and J. Wolf. Transient response of ISOPHOT Si:Ga infrared photodetectors: experimental results and application of the theory of nonstationary processes. *Proceedings of SPIE*, 2553:461–469, September 1995.
37. J. Schubert, G. Roth, J. Wolf, D. Lemke, and B. I. Fouks. Correction and curing of in-orbit-induced nonideal behavior of ISOPHOTS's photodetectors. *Proceedings of SPIE*, 2268:283–294, September 1994.
38. J. See. Correction des effets mémoire de l'instrument ISOPHOT C-100. Technical report, Stage de magistère, 1999.
39. H. W. Sorenson. *Parameter estimation*, volume 9 of *Control and system theory.* Marcel Dekker, Inc., New-York and Basel, 1980.
40. J.-L. Starck et al. Faint source detection in ISOCAM images. *Astron. Astrophys. Suppl. Ser.*, 138:365–379, August 1999.
41. D. Tiphène, D. Rouan, G. Epstein, and P. Le Coupanec. Modelling transient effects in the IR array of the short wavelength channel of ISOCAM, the camera onboard the ISO satellite. *accepted in Experimental Astronomy*, May 1999.
42. L. A. Vinokurov and B. I. Fouks. Spreading of the current in a photosensitive medium exhibiting an extrinsic photoconductivity. *Sov. Phys. Semicond.*, 22(11):1258–1262, November 1988.
43. L. A. Vinokurov and B. I. Fouks. Nonlinear photoresponse of extrinsic photoconductors. *Sov. Phys. Semicond.*, 25(11):1207–1211, November 1991.
44. L. A. Vinokurov, N. B. Zaletaev, V. F. Kocherov, and B. I. Fouks. Spreading of time dependent photocurrrent in Si:Ga. *Sov. Phys. Semicond.*, 26(4):433–435, April 1992.
45. J. W. Wensink et al. Characteristics of the ISO Short-Wavelength Spectrometer detectors. In *ESA SP-356 Photon Detectors for Space Instrumentation*, pages 339–344, December 1992.
46. J. Wolf. Low-background far-infrared detectors and arrays. *Optical Engineering*, 33(5):1492–1500, May 1994.